Laser induced deposits in contaminated vacuum environment: Optical properties and lateral growth

Frank R. Wagner, Georges Gebrayel El Reaidy, Delphine Faye, Jean-Yves Natoli

TITLE
Laser induced deposits in contaminated vacuum environment: optical properties and lateral growth

Authors
Frank R. WAGNER[a], Georges GEBRAYEL EL REAIDY[a,b], Delphine FAYE[b], Jean-Yves NATOLI[a]

Corresponding author
Frank R. WAGNER[a]

e-mail adresses
frank.wagner@fresnel.fr, reaidy@fresnel.fr, delphine.faye@cnes.fr, jean-yves.natoli@fresnel.fr

Affiliations
[a]Aix Marseille Univ, CNRS, Centrale Marseille, Institut Fresnel, Marseille, France
[b]Centre National d'Etudes Spatiales, 18, Avenue E. Belin – 31401 Toulouse Cedex 9, France

Abstract
The lifetime of high power photonics instruments operating in vacuum is often strongly reduced due to an effect designated as Laser Induced Contamination (LIC): Outgassing from polymers generates molecular contamination on the optical components and the interaction between the laser beam and the contaminants induces the growth of an often carbonaceous deposit. The LIC deposit then partly absorbs the laser pulses which leads to fast reduction of the instrument performances.
In this study, we generated LIC deposits using a nanosecond laser at 355 nm. Toluene and the outgassing products from an epoxy adhesive are used as contaminants. We then analyzed the optical properties of different zones of the 100 µm large and 10 nm thick deposit using advanced optical techniques. These data will be useful for numerical simulations of the deposit evolution. We also investigated the mechanism of the lateral growth of the crater-shaped deposit and found strong indications that heat conduction from the center of the deposit sustains the lateral growth into regions where the local fluence is small.

Keywords
1. Laser induced contamination
2. Toluene
3. Tripled Nd:YAG laser
4. Light induced deposit
5. Optical properties
6. Lateral crater growth mechanism

1. Introduction

Contamination-induced optical damage in sealed laser systems was first reported in 1994 [1], but is still a critical issue in present high performance laser systems [2,3]. Roughly, outgassing of polymers causes organic contamination on optical components where photo-polymerization by the laser irradiation takes place. Ongoing irradiation of the contamination-based deposit then often leads to catastrophic laser-induced damage at fluences that are safe in open laser systems. The whole process is similar to light-induced (or light-enhanced) chemical vapor deposition (LICVD) and appears even more easily in vacuum environments [4].

Already the formation of the contamination-based deposit is considered as "damage" according to the official definition of laser-induced damage as "any permanent light-induced modification…" [5].

In fact, even if irradiating the deposit does not lead to a plasma and thus micro-cracks or other mechanical damage, the deposit was shown to significantly reduce the transmission of the optical component [6].

Today, most investigations on *laser-induced (molecular) contamination* (LIC or LIMC), as the process is also named [7,8], are conducted in the framework of specific space missions. In fact, the space industry identified it as a major risk for its high power photonics instruments [9–11,7]. In future, in order to reduce the number of costly experimental LIC validations of the instrument design, one would like to be able to model the LIC effect. For modeling however, more systematic knowledge on the deposition process and on the properties of the deposits are necessary.

The deposition process starts with a deposit morphology that reproduces the fluence distribution of the laser beam on the sample [7,11]. For nanosecond pulsed lasers, the morphology of the deposit then evolves into a laterally growing crater-like shape for higher pulse numbers or higher fluences [7,11]. This means that at a given location on the sample, the deposit will first increase in thickness (phase 1) and later decrease (phase 2), before, sometimes, plasma-related damage is observed (phase 3).

Depending on the contamination (playing the role of a LICVD precursor) the LIC deposits can occur more or less easily and have more or less strong impact on light propagation [1,12]. Lately, naphthalene-based deposits (3×10^{-4} hPa) generated by 355 nm irradiation (0.5-2.4 J/cm^2) of uncoated quartz samples have been used to develop an empirical model for the temporal evolution of the caused transmission loss. In fact, naphthalene is known for causing quickly strongly absorbing LIC deposits [1] thus Kokkinos *et al.* approximated the transmission of the deposit by an opaque disk at the beam center that increases in size over time blocking more and more of the incident light [13]. Hence, this model is valid for heavy contamination alongside with localized laser damage sites that completely absorb or diffuse the center part of the incident beam.

Our aim for this study is to work with more representative contaminants observed in spatial applications (toluene and outgassing of an epoxy-based adhesive) and deposits causing less severe transmission loss (< 5%). After the illustration that these LIC deposits can act as an optical interference coating [14,15] we can now go a step further and deduce real and imaginary part of the refractive index for the different zones of the deposit (outside the crater, inside the crater). We further want to show that a thermal effect in the lateral growth mechanism cannot be neglected for our experimental conditions.

2. Material and methods

Our vacuum chamber has been described in detail elsewhere [14]. Briefly, the sample is located at the center of the chamber and the inner window surfaces are at a distance of approximately 70 mm from the sample surfaces. The laser beam, transmitted by the entrance window, the sample and the exit window, is focused onto the sample to keep the fluence on the windows at low values, thus avoiding LIC deposits on the windows. The test material, either toluene or epoxy adhesive, is located in a smaller secondary chamber being connected with the main chamber by a short tube and a regulation valve. All parts are separately temperature controlled and an active carbon filter is installed in the exhaust line.

Close to the recommendations of the ISO standard [8] we clean the chamber after each test with a bake-out at 170°C followed by a blank test. Additionally to the in-situ measurements described

below, the absence of any deposit after the blank test is checked by inspection with a scanning white light interferometer (Zygo NewView 7300). Good reproducibility has been obtained with this experimental protocol [14].

We use a frequency tripled Nd:YAG laser (Quantel YG980) at 355 nm delivering longitudinal multi-mode pulses with a FWHM pulse duration of 13 ns at a pulse repetition rate of 10 Hz. During the irradiation, beam splitters sending part of the beam onto calibrated photodiodes before and after the vacuum chamber allow to measure the transmission of the irradiated site and a cooled CCD camera (Hamamatsu ORCA-ER-1394) records the photoluminescence of the sample through a low pass filter [14].

The used epoxy adhesive is gray EC-2216 (3M Scotch-Weld) and its outgassing species have been characterized by gas chromatography mass spectrometry (GC-MS) showing an important contribution of toluene (Figure 1). The LIC tests were performed with approximately 1 g of polymerized adhesive in the shape of a 1 mm thick plate (without pre-bake-out).

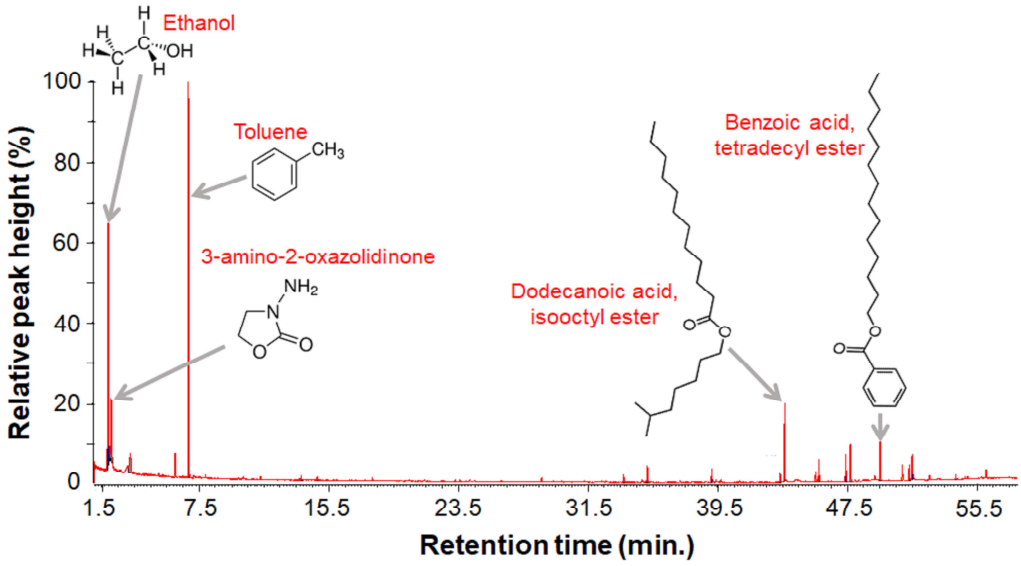

Figure 1: Gas chromatography mass spectrometry characterization of gray EC-2216 epoxy adhesive at 115°C. Toluene is an important part of the resulting molecular contamination.

Due to the focused laser beam, the deposits obtained in our setup are only 60 – 180 µm in diameter. Considering that the deposits are also less than 10 nm high, determining real and imaginary part of the refractive index (respectively n and κ), in particular distinguishing the zones inside and outside the crater, needs tools with good lateral resolution and sensitivity. The characterization tools should also avoid alteration of the nanoporous [14,15] and probably carbonaceous [16], organic deposits. We use scanning white light interferometry (SWLI) (Zygo NewView 7300) for measuring the physical thickness d and quadriwave lateral shearing interferometry (QLSI) (Phasics Sid4Bio) for the measurement of relative transmission T and relative optical path difference OPD [17]. In order to measure T and OPD, the QLSI software compares the zone with the LIC deposit to a nearby reference zone without deposit. The measurements of d, T and OPD are thus all obtained by low intensity irradiation in imaging devices minimizing the risk of altering of the deposits during the measurement. After treating the SWLI measurement for background subtraction in Gwydion [18] we use ImageJ [19]

with the Sync Windows plugin [20] to select lines in the different zones of the deposit for which all properties are more or less constant retrieving in this way *d*, *T* and *OPD* values with their uncertainties for each zone. Considering the LIC deposit in each zone as a homogeneous dielectric material, we can then search for the best value of the complex refractive index of the deposit being compatible with the measurements. As even for an uncoated substrate the solution has to be found numerically [21], we directly implemented the transfer matrix formalism which can be extended to a coated substrate [22].

For estimating the dispersion of *n* and κ, the QLSI camera was mounted on a microscope equipped with a set of LEDs allowing us to measure the optical properties of the LIC deposit at ten different wavelengths [21].

3. Results and discussion

3.1. Optical characterization of toluene-based deposits

Figure 2 (a), (c) and (e) shows images of *d*, *T* and *OPD* where the latter two are measured with a wavelength of 780 nm. The substrate is super-polished synthetic fused silica and the contaminant was toluene at a pressure of 0.1 hPa. The laser delivered 180'000 pulses (5 hours of irradiation at a pulse repetition rate of 10 Hz) with a peak fluence of 0.47 J/cm^2. Figure 2 (b), (d) and (f) show cross sections of homogeneous zones in these images. The zones were chosen to be representative for the different phases of the deposit evolution: Zones 2 and 3 are outside the crater and are representative for growth phase 1 during which the deposit thickness increases. Zone 1 is inside a forming crater and is representative for phase 2 during which the deposit thickness ins decreasing. Finally, zone 4 is the reference of the substrate without LIC deposit.

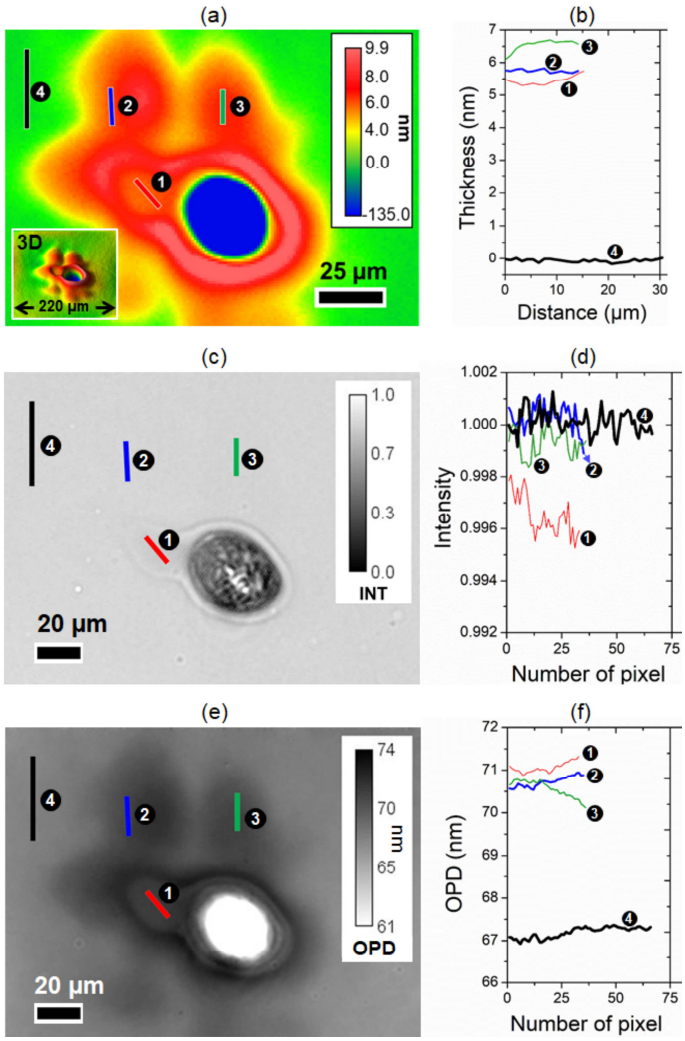

Figure 2: Deposit thickness d (figures (a) and (b)), transmission T (figures (c) and (d)) and optical path difference OPD (figures (e) and (f)). Transmission and optical path difference are for 780 nm wavelength light. The figures (b), (d) and (f) show cross sections of homogeneous zones 1-4 indicated by black lines in figures (a), (c) and (e). The zones are: 2. and 3. are outside the crater (growth phase 1), zone 1 is in inside a forming crater (growth phase 2), finally zone 4 is the background reading. Contamination was 0.1 hPa of toluene and irradiation was performed with 180'000 pulses with a peak fluence of 0.47 J/cm^2.

It has been shown before that the beginning of LIC-deposit formation on uncoated substrates is accompanied by a transmission increase of the laser beam [14,15,23]. We also showed that epoxy-adhesive based deposits show varying transmission when varying the observation wavelength [15]. Both of these observations indicate that the deposit can be treated as a lossy optical interference layer and we used the method described above to retrieve the local optical properties of the deposited material. The statistical uncertainty in the complex refractive index retrieved by this method, which is arising from the distribution of the values in Figure 2 (b),(d),(f), is low as the 68% error bars barely stand out from the symbols used to plot the mean values in Figure 3.

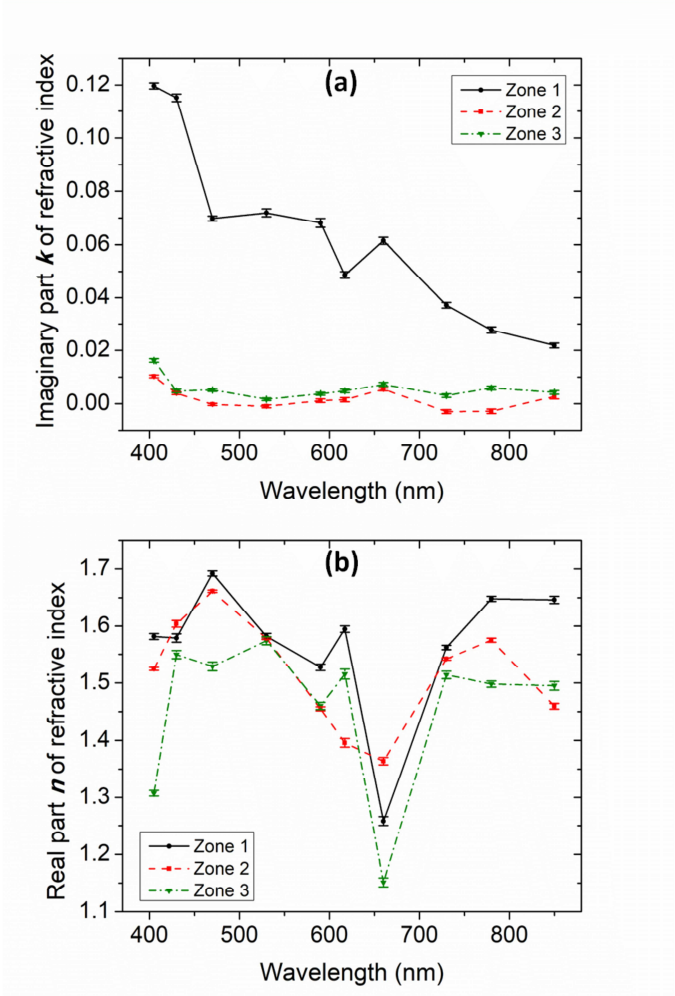

Figure 3: (a) Imaginary part and (b) real part of the refractive index for the different zones of the deposit. Zone 1 is inside a forming crater (representative for growth phase 2). Zone 2 and 3 are outside of the crater (representative for growth phase 1).

Zone 1, inside the forming crater, is clearly much more absorbing than zones 2 and 3 outside the crater that give essentially identical results. Approximating $\kappa_1 \approx 0.07$ at 550 nm, the corresponding absorption coefficient is $\alpha = 1.6 \times 10^4$ cm^{-1}, whereas outside the crater we obtain only 2.5% of this value. We should now compare these values to known absorption coefficients for soot or other carbonaceous decomposition products which are at least 5.7×10^4 cm^{-1} for similar wavelength [24]. It is thus clear that even the deposit inside the crater cannot be considered as soot. The deposit outside the crater is only very weakly absorbing. This is in part due to its nanometric porosity [15] but also an incomplete chemical dissociation of the toluene molecules.

The refractive index values of all zones vary rapidly with wavelength and can be for some wavelengths lower that the index of the substrate (≈1.45). This weak refractive index can be better understood considering the nanometric porosity of the deposit previously observed in this zone [15]. It is, together with the weak absorption, at the origin of the transmission increase observed at the onset of the LIC deposit formation on bare substrates [14].

3.2. Lateral growth beyond the laser beam size

It has been reported before that, in conditions where a crater-shaped deposit is obtained, the crater is larger for the same pulse number if the peak fluence is higher, even though the rim height of the crater is constant [7,11]. In their deposition conditions, Schroeder *et al.* could in fact relate the crater diameter to the size of the Gaussian laser beam on the sample because the local fluence at the crater rim was constant. The observed size difference after a given irradiation time (Figure 4) is caused by a lateral growth during the irradiation as has been shown by in-situ fluorescence measurements [7,11,14]. In fact, all deposits start with a small bump at the position of maximum fluence. The bump evolves into a crater and the crater grows mostly laterally until the end of the irradiation.

Figure 4(a)-(e) show a series of SWLI measurements performed on LIC deposits obtained after the same number of pulses with the same laser beam profile (Fig. 4(f)) but using different peak fluences.

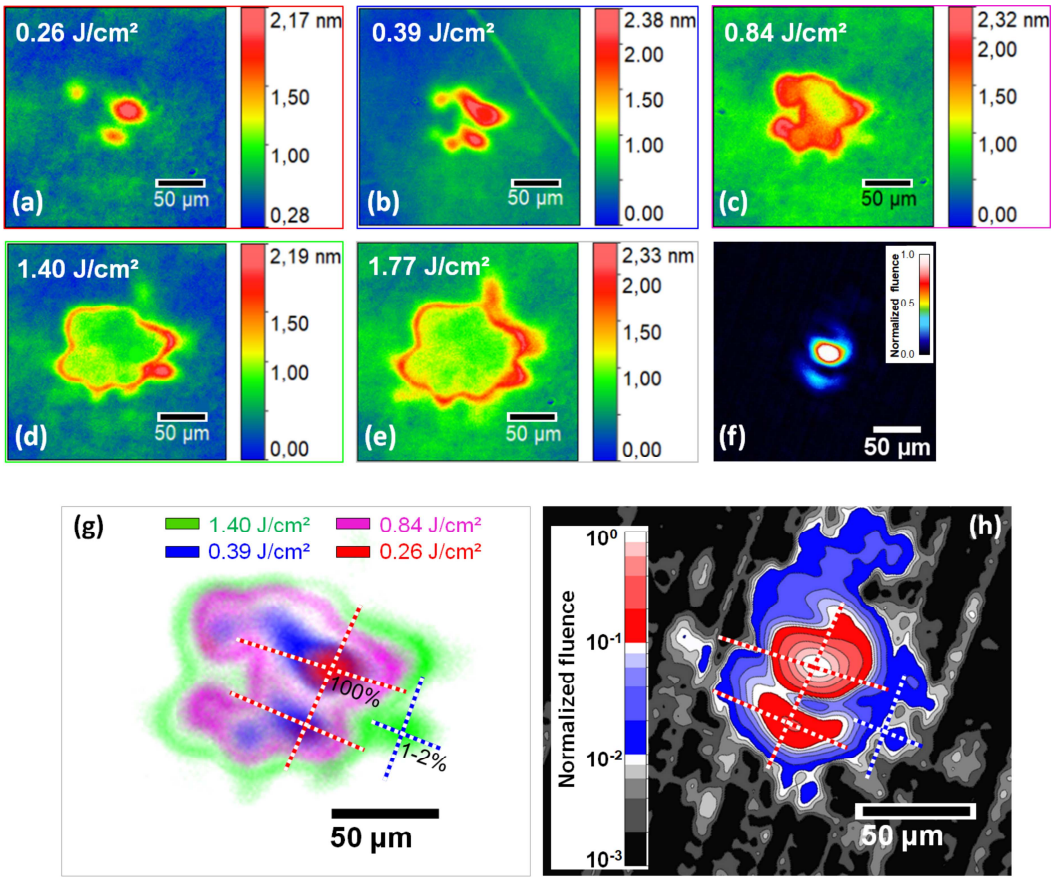

Figure 4: (a)-(e) SWLI measurements performed on LIC deposits obtained after the same number of pulses with the same laser beam profile and the same contamination, but using different peak fluences. (g) The measurements (a)-(d) in monochrome color coding (transparent to saturated) superposed to measure the distance from the beam center to the characteristic satellite on the right side of measurement (d). (h) and (f) Representations of the local fluence distribution of the sample in logarithmic (h) and linear (f) fluence scale. For better size comparison (f) is at the same scale as the deposits in (a)-(e). (Deposition conditions: 1g of epoxy adhesive EC2216 outgassing at 100°C, 540'000 laser pulses on sample with an HfO2 monolayer.)

Aligning the laser beam profile (h) and (f) with the shape of the deposit obtained at small peak fluence (a) and superposing all deposit measurements (g) allow to identify the local fluence at the

characteristic satellite appearing on the right side of the deposit at higher fluence (d). The result of this measurement is that the local fluence at the characteristic satellite is only between 1% and 2% of the peak fluence. For a peak fluence of 1.4 J/cm^2 (d), this translates to a local fluence of less than 0.028 J/cm^2 at the position of the characteristic satellite that reaches the same height after the same number of pulses in the same contamination conditions as the deposit at the center of the beam at 0.26 J/cm^2 (a). Hence, two more or less identical deposits are obtained at local fluences differing by a factor of ten.

The lateral growth of the deposit can be quantified in terms of the surface covered by the deposit, *A*, as function of peak fluence *F* (Figure 5). The deposit surface grows linearly with the peak fluence, which has been observed for different outgassing temperatures (60°C and 100°C) and HfO_2-coated and uncoated SiO_2 substrates.

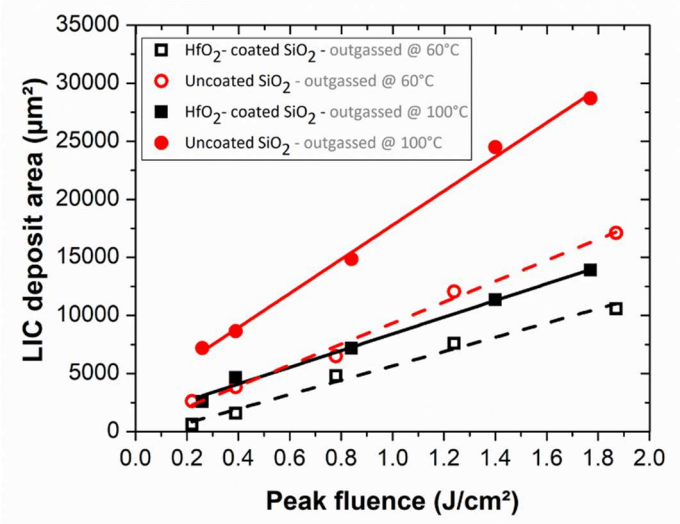

Figure 5: Surface covered by the LIC deposit in different experimental conditions as function of the peak fluence of the laser beam. The contaminants are always the outgassing of 1g of epoxy adhesive and the laser pulse number is always 540'000. For comparison, the effective surface of the laser beam is 2520 µm^2.

From these observations we can conclude that the local fluence is not the only parameter influencing the growth of a LIC deposit. In order to explain the lateral expansion of the deposit to locations "far" away from the beam center, we can use our characterizations of the optical properties of the deposit. Indeed, the inner part of the crater becomes rather absorbing. Absorption of the light will then cause a temperature rise (which has been quantified for naphthalene deposits to reach 1500K [25]). We thus hypothesize that the LIC deposition process, at least "far" away from the beam center, is driven by the local fluence as well as thermal energy provided by the center of the deposit through heat conduction.

Naturally the thermal energy that can contribute to the deposition process is more important when the peak fluence is higher. Thus, when using high fluence irradiation, the deposit can grow to sizes that are much larger than the laser beam.

The transient temperature rise at the beam center can be rather high and may cause local plasma ignition leading to microscopic damage of the substrate. Whether or not damage (void formation) in the substrate occurs, depends on the peak fluence and the pulse number but also on the

contamination: For 0.1 hPa of toluene we observed substrate damage for fluences larger than 0.5 J/cm^2 and 180'000 pulses [14], whereas for outgassing of 1g of epoxy adhesive (at 60°C and at 100°C) we did not observe any substrate damage using up to 1.8 J/cm^2 and 540'000 pulses.

4. Summary and Conclusions

In this paper we studied laser-induced deposits on optical surfaces. These deposits are generated due to nanosecond 355 nm laser irradiation of the optics in a contaminated vacuum environment as it occurs typically in satellites. We used two types of molecular contamination: 0.1 hPa of toluene and the outgassing products of an epoxy adhesive.

We characterized the optical properties of different zones of the deposit in the stage where the deposit takes the shape of a crater (also named "donut" in literature). The method used for the characterization is based on the measurement of the physical heights of the deposits using optical profilometry (scanning white light interferometry) as well as on the measurement of the local and wavelength dependent relative transmission and optical path difference acquired by a QLSI-camera (quadriwave lateral shearing interferometry). Considering the deposits as vertically homogeneous we then presented wavelength dependent data of the complex refractive index for the deposit inside a forming crater and two zones outside the crater. The deposit inside the crater was found to be rather absorbing (but not as absorbing as soot), whereas the deposit in the two zones outside the crater was only very weakly absorbing. This weak absorption, combined with low refractive index due to nanometric porosity in this zone, is at the origin of the transmission increase observed on uncoated substrates at the onset of the deposition process [14,15].

We also reported on the lateral growth behavior of the crater-shaped deposits as function of peak fluence. In our experimental conditions, the surface covered by the deposit grows linearly with the peak fluence of the beam. The final surface of the deposit can extend to locations where the local fluence is very small. We observed practically the same deposit thickness for 0.26 J/cm^2 at the center of the beam and for 0.028 J/cm^2 at a recognizable position at some distance from the beam center. Since the inside of the crater-shape is absorbing and was irradiated in the latter experiment with a peak fluence of 1.4 J/cm^2, we propose to explain the lateral growth of the crater into regions of small local fluence by heat conduction from the deposit center to the periphery.

In conclusion, future modeling of the LIC process has to take into account not only the local fluence but also the temperature distribution, which is linked to the shape of the full beam, its pulse energy and the properties of the irradiated materials. One necessary input for the calculation of the temperature distribution, the absorption coefficients of the deposit inside and outside the crater, is also given in this paper.

Funding:

This work was supported by the Centre National d'Etudes Spatiales (CNES) and Airbus Defense and Space (ADS) through the PhD grant of Georges GEBRAYEL EL REAIDY [grant number 2585].

References

[1] F.E. Hovis, B.A. Shepherd, C.T. Radcliffe, A.L. Bailey, W.T. Boswell, Optical damage at the part per million level: the role of trace contamination in laser-induced optical damage, in: Laser-Induc.

Damage Opt. Mater. 1993, International Society for Optics and Photonics, 1994: pp. 145–153. doi:10.1117/12.180872.
[2] P. Zhang, Y. Jiang, J. Wang, W. Fan, X. Li, J. Zhu, Improvements in long-term output energy performance of Nd:glass regenerative amplifiers, High Power Laser Sci. Eng. 5 (2017). doi:10.1017/hpl.2017.24.
[3] H. Hong, Q. Liu, L. Huang, M. Gong, Improvement and formation of UV-induced damage on LBO crystal surface during long-term high-power third-harmonic generation, Opt. Express. 21 (2013) 7285–7293.
[4] X. Ling, Y. Zhao, D. Li, S. Li, M. zhou, J. Shao, Z. Fan, Impact of organic contamination on the laser-induced damage in vacuum, Appl. Surf. Sci. 255 (2009) 9255–9258. doi:10.1016/j.apsusc.2009.07.012.
[5] International Organization for Standardization, Determination of laser-damage threshold of optical surfaces Part 1: 1-on-1 test, ISO 11254–1 (2000).
[6] H. Schröder, P. Wagner, D. Kokkinos, W. Riede, A. Tighe, Laser-induced contamination and its impact on laser damage threshold, in: Laser-Induc. Damage Opt. Mater. 2013, International Society for Optics and Photonics, 2013: p. 88850R. doi:10.1117/12.2030002.
[7] W. Riede, H. Schroeder, G. Bataviciute, D. Wernham, A. Tighe, F. Pettazzi, J. Alves, Laser-induced contamination on space optics, in: Laser-Induc. Damage Opt. Mater. 2011, SPIE, 2011: p. 81901E.
[8] International Organization for Standardization, Optics and photonics - Lasers and laser-related equipment - Laser-induced molecular contamination testing, ISO 20811:2017 (2017).
[9] J.B. Abshire, X. Sun, H. Riris, J.M. Sirota, J.F. McGarry, S. Palm, D. Yi, P. Liiva, Geoscience Laser Altimeter System (GLAS) on the ICESat Mission: On-orbit measurement performance, Geophys. Res. Lett. 32 (2005). doi:10.1029/2005GL024028.
[10] D. Wernham, A. Ciapponi, W. Riede, P. Allenspacher, F. Era, A. D'Ottavi, D. Thibault, Verification for robustness to laser-induced damage for the Aladin instrument on the ADM-Aeolus satellite, in: Laser-Induc. Damage Opt. Mater. 2016, International Society for Optics and Photonics, 2016: p. 1001408. doi:10.1117/12.2245545.
[11] H. Schröder, S. Borgmann, W. Riede, D. Wernham, Investigation of laser induced deposit formation under space conditions, in: CNES / ESA, Toulouse, 2008. https://atpi.eventsair.com/QuickEventWebsitePortal/icso-proceedings/info/ExtraContent/ContentSubPage?page=1&subPage=5 (accessed May 20, 2019).
[12] F.E. Hovis, B.A. Shepherd, C.T. Radcliffe, H.A. Maliborski, Mechanisms of contamination-induced optical damage in lasers, in: Laser-Induc. Damage Opt. Mater. 1994, International Society for Optics and Photonics, 1995: pp. 72–83. doi:10.1117/12.213736.
[13] D. Kokkinos, H. Schroeder, K. Fleury-Frenette, M.P. Georges, W. Riede, G. Tzeremes, P. Rochus, Laser optics in space failure risk due to laser induced contamination, CEAS Space J. 9 (2017) 153–162. doi:10.1007/s12567-016-0137-1.
[14] G.G. El Reaidy, F.R. Wagner, D. Faye, J.-Y. Natoli, Study of the first stages of laser-induced contamination, Opt. Eng. 57 (2018) 121903. doi:10.1117/1.OE.57.12.121903.
[15] G.G. El Reaidy, F.R. Wagner, D. Faye, J.-Y. Natoli, Laser-induced contamination (LIC): anti-reflective effect of early stage deposits, in: Laser-Induc. Damage Opt. Mater. 2018 50th Anniv. Conf., International Society for Optics and Photonics, 2018: p. 108051K. doi:10.1117/12.2500081.
[16] W. Riede, P. Allenspacher, H. Schröder, D. Wernham, Y. Lien, Laser-induced hydrocarbon contamination in vacuum, in: Laser-Induc. Damage Opt. Mater. 2005, International Society for Optics and Photonics, 2006: p. 59910H. doi:10.1117/12.638765.
[17] P. Bon, G. Maucort, B. Wattellier, S. Monneret, Quadriwave lateral shearing interferometry for quantitative phase microscopy of living cells, Opt. Express. 17 (2009) 13080–13094. doi:10.1364/OE.17.013080.
[18] Gwyddion – Free SPM (AFM, SNOM/NSOM, STM, MFM, …) data analysis software, http://gwyddion.net/ (accessed June 19, 2019).
[19] ImageJ, https://imagej.nih.gov/ij/ (accessed June 19, 2019).

[20] ImageJ: Sync Windows plugin for ImageJ, https://imagej.net/Sync_Windows (accessed June 20, 2019).
[21] S. Khadir, P. Bon, D. Vignaud, E. Galopin, N. McEvoy, D. McCloskey, S. Monneret, G. Baffou, Optical Imaging and Characterization of Graphene and Other 2D Materials Using Quantitative Phase Microscopy, ACS Photonics. 4 (2017) 3130–3139. doi:10.1021/acsphotonics.7b00845.
[22] O.S. Heavens, Optical properties of thin films, Rep. Prog. Phys. 23 (1960) 1–65. doi:10.1088/0034-4885/23/1/301.
[23] M. Liessmann, L. Jensen, I. Balasa, M. Hunnekuhl, A. Buttner, P. Wessels, J. Neumann, D. Ristau, Scaling of Laser-induced Contamination Growth at 266 nm and 355 nm, in: Laser-Induc. Damage Opt. Mater. 2015, SPIE, 2015: p. 96321Z.
[24] M.R. Querry, D.& E.C. (U. S.) Chemical Research, United States, M. and C.C. Army Armament, Optical constants of minerals and other materials from the millimeter to the ultraviolet, US Army Armament, Munitions & Chemical Research, Development & Engineering Center, Aberdeen Proving Ground, Md., 1987.
[25] D. Kokkinos, P. Gailly, M.P. Georges, G. Tzeremes, P. Rochus, K. Fleury-Frenette, Real-time measurement of temperature variation during nanosecond pulsed-laser-induced contamination deposition, Appl. Opt. 54 (2015) 10579–10585. doi:10.1364/AO.54.010579.